ARTICLE

Enhancement in Room Temperature Ammonia Sensing Properties of Naphthalene Diimides through Core Expansion

Received 00th January 20xx,
Accepted 00th January 20xx

DOI: 10.1039/x0xx00000x

Salman Ali,[a] Mohammed A. Jameel,[a] Glenn Oldham,[a] Akhil Gupta,[a] Mahnaz Shafiei,*[a] and Steven J. Langford*[a,b]

Abstract: An amperometric type sensor whose active layer is derived from a tetra core-substituted organic semiconductor, naphthalene diimide (NDI-CN_4), has been evaluated for ammonia gas (3, 6, 25 and 50 ppm) sensing at room temperature against the parent NDI devoid of core-substitution effects. In empirical terms, the tetracyano derived sensor showed high sensitivity (178% at 50 ppm NH_3) and selectivity, quick response and recovery (12.5 s/39 s), low limit of detection (3 ppm), and importantly, excellent recyclability and stability. Density functional theory and cyclic voltammetry studies indicate that the incorporation of strong electron-withdrawing groups, i.e. cyano groups, cause a substantial decrease in the reduction potential of the NDI-CN_4 leading to a significant rise in the current of sensor, mainly due to an efficient charge-transfer between NDI-CN_4 and ammonia. Furthermore, because of low-lying LUMO energy level, the NDI-CN_4-based sensor shows high stability even with prolonged exposure to ambient air. A comparison with the corresponding core-unsubstituted NDI derivative confirms the positive cooperative effect of core-cyanation on gas sensing performance. It is anticipated that this work could give some useful information for preparing high performance organic sensing devices.

Keywords: Naphthalene diimide, core substitution, ammonia sensing, low LUMO level, high stability.

1. Introduction

Ammonia is a critical commodity chemical with extensive applications in fertilisers, synthetic fibres, drugs, and plastics manufacturing, but it is a highly corrosive and poisonous gas that can propagate into the environment.[1] Moreover, ammonium salts such as ammonium nitrate (NH_4NO_3) are found in various explosives and slowly dissociate to release trace amounts of ammonia that need to be detected and monitored to avoid accidents such as the August 2020 Lebanon explosion which killed 220 people and left over 300,000 homeless.[2] Though ammonia has applications in numerous research areas, its exposure in high concentrations is deadly to humans, leading to prolonged effects based on edema and airway destruction, through burning. The lower limit of human perception by smell is around 50 ppm for ammonia.[3] However, even underneath this limit, it is irritating to skin, eyes, and respiratory system, potentially leading to a persisting cough and nose/throat irritation.[4] Additionally, ammonia exists in the respired breath in humans, which may act as a potential indicative biomarker for various kinds of kidney disorders and hepatitis. Thus, detection through respiratory tests is vital for treatment strategies.[5] The permissible limits of ammonia exposure in the human body are 25 ppm over an 8 hour period and 35 ppm over a 10 minute period, and are advised and legislated by The Health and Safety Executive (HSE), London.[6]

There have been numerous investigations on ammonia sensing based on metal oxides,[7-9] conducting polymers,[10, 11] carbon nanotubes,[12, 13] graphene-based materials[14] and small organic molecules,[15] and all have their advantages and disadvantages. Among numerous small organic semiconductor materials, we and others have been exploring the naphthalene diimide derivatives (NDIs) in the field of organic electronics due to their conducting and thermal features.[16, 17] Due to the presence of their π-conjugation, they can also be utilised as potential sensing materials for detecting desired species after variations at either the imide position (i.e. a longitudinal position) or core position (i.e. a lateral position) with appropriate functional groups (Fig. 1).[18, 19] The dyestuffs achieved through imide substitution usually have similar absorption and emission properties as the effect of such substitution on the electronics of the NDI is low, so such positions hold a processing functionality only. Through core-substitution strategies, NDI derivatives with desired electronic and photonic properties can be achieved.[20] For example, attaching electron-withdrawing groups such as nitrile,[21] fluoro,[22] and chloro groups[23] to the conjugated core leads to a concomitant drop in the lowest unoccupied molecular orbital (LUMO) energy level thereby allowing the efficient injection of electron carriers by reducing the charge injection barrier. We surmise this should lead to an enhancement in the performance of

[a] School of Science, Computing and Engineering Technologies, Swinburne University of Technology, Hawthorn Victoria 3122 Australia.
[b] School of Mathematical and Physical Sciences, University of Technology Sydney, Ultimo NSW 2007 Australia
*Corresponding authors: mshafiei@swin.edu.au; steven.langford@uts.edu.au

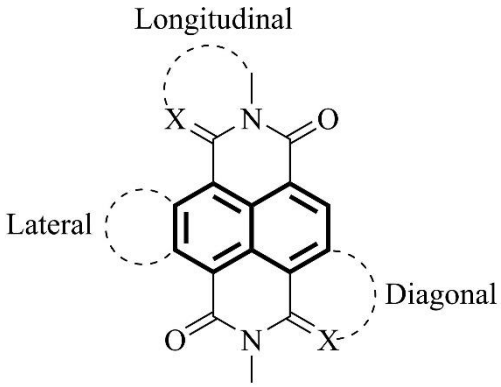

Fig. 1 NDI functionalisation occurs in three distinct ways.

chemical sensors demonstrated to date in terms of sensitivity and air stability.[24] Their solution processability, easy of synthesis and ability to be highly purified make them promising candidates for the development of high-performing sensors. However, despite these desirable features, a very little attention has been paid to NDIs in electrically-transduced sensors (amperometric, resistive and capacitive).[18, 25] To this end, we recently began a systematic study to investigate the effect of functionalisation of NDI derivatives carrying different hydrophilic and hydrophobic groups at imide side for potential applications in humidity and ammonia sensing.[26, 27] The results revealed that different functional groups on the imide position affect surface morphology and crystallinity and interact differently in the presence of water and ammonia in a measurable way.

Ambient stability signifies one critical parameter that controls the performance and pragmatism of organic electronic devices. Because certain species are present in the ambient air, such as oxygen, they can easily diffuse into organic materials and destabilise or trap the negative charge carriers in the channel. As a result, most n-type organic semiconductors including NDIs described in the current literature lack the necessary stability under ambient conditions.[28] As we have already mentioned, ambient stability can be accomplished by reducing the LUMO energy level and improving solid-state packing modes.[21, 22] Thus, some studies for the effect of core-substituted groups on ambient stability need to be performed to offer guidance and appropriate design characteristics for further development of high-performing NDI-based gas sensors.

In this work, two NDI derivatives, the core-substituted NDI-CN_4 and unsubstituted NDI-H_4 (Fig. 2a and b), have been synthesised and their ammonia gas sensing properties have been investigated and compared. This work mainly focuses on the effect of electron-withdrawing group (CN) on ammonia sensing performance of NDI derivative described through evaluation of sensitivity, selectivity, response and recovery time, limit of detection (LOD), and long-term stability.

2. Materials and Methods

2.1 Synthesis

Synthesis of NDI-CN_4 and NDI-H_4 (Fig. 1) was carried out using the published procedures.[29, 30] NMR spectra are presented in the Supplementary Information (SI).

NDI-CN_4: A dark blue powder (m.p. = 274 °C); ^{1}H NMR (400 MHz, $CDCl_3$) δ 4.34 – 4.25 (m, 4H), 1.85 – 1.72 (m, 4H), 1.48 – 1.16 (m, 20H), 0.94 – 0.79 (m, 6H); λ_{max} = 578 nm.

NDI-H_4: An off-white solid with metallic lustre (m.p. = 184 °C); ^{1}H NMR (400 MHz, $CDCl_3$) δ 8.76 (s, 4H), 4.22 – 4.16 (m, 4H), 1.74 (dt, *J* = 15.3, 7.5 Hz, 4H), 1.47 – 1.21 (m, 20H), 0.87 (t, *J* = 6.9 Hz, 6H); λ_{max} = 368 nm.

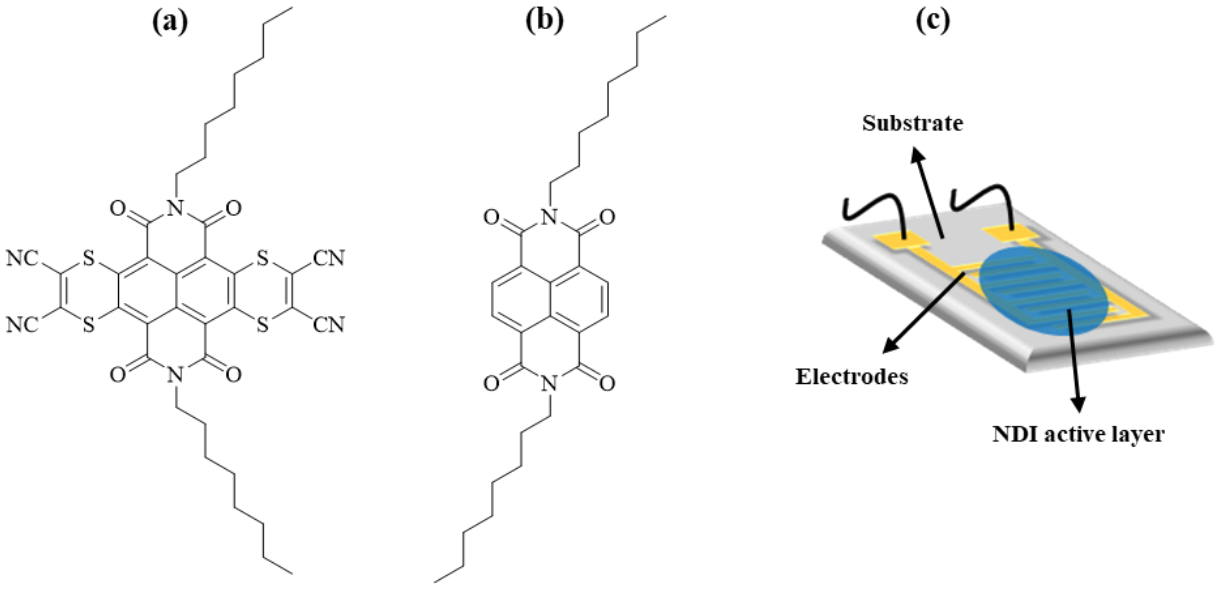

Fig. 2 Chemical structures of (a) NDI-CN_4, (b) NDI-H_4 and (c) Device structure.

2.2 Thin Film Sensor Fabrication

Silicon (Si) substrates and interdigitated electrodes (IDEs) were utilised in the preparation of thin films and sensors, respectively. The IDEs (10 mm × 6 mm × 0.75 mm dimensions with 10 µm spacing between the fingers) were acquired commercially from Micrux Technologies and consist of a quartz (SiO_2) substrate patterned with gold (Au) electrodes. The Si substrates and IDEs were washed by sonicating in isopropanol and acetone followed by deionised water. The IDEs were dried over nitrogen gas and were kept in an oven at 80 °C overnight to dry out any remaining contaminations. Solutions (10 mg/mL) of NDI-CN_4 and NDI-H_4 in tetrahydrofuran (THF) were prepared and spin-coated over the substrates at 2000 rpm for one min. The prepared films were kept at room temperature for 2 h to eliminate any residual solvent.

2.3 Measurements

Gas sensing studies of the fabricated sensors were conducted at 24±0.5 °C in a custom-built, fully automated multi-channel gas calibration system consisting of six mass flow controllers (MFCs) and a LINKAM HFS600E chamber and RH95 humidity generator in which humidity is controlled through synthetic air. Certified gas cylinders of high purity (99.999%) dry synthetic air and low concentrations of target gases such as: 50 ppm ammonia, 12 ppm nitrogen dioxide, 50 ppm hydrogen and 50 ppm acetone balanced in synthetic air were used. The concentration of the analyte gases is diluted with synthetic air by adjusting the flow rates of each MFCs while maintaining a total constant flow rate of 200 sccm. The gas sensing response was recorded by a Keithley picoammeter at a constant bias voltage of 5 V. Sensitivity was evaluated using $S=\Delta I/I_o$ where S represents sensitivity, ΔI is a change in sensor current after exposure to a target gas, and I_o is the current in the air. Surface morphology of the prepared thin films was studied employing atomic force microscopy (AFM), operated in a semi tapping mode at 0.79 Hz. X-ray diffraction (XRD) analysis was conducted through Bruker Advanced X-ray Solutions D8 at 40 kV, 40 mA with CuKα radiation (λ = 0.154 nm). Thermogravimetric analysis (TGA) was conducted using a Q-500 TGA apparatus with nitrogen as a purging gas. Samples were heated up to 700 °C at 10 °C/min under a nitrogen atmosphere. Differential scanning calorimetry (DSC) analysis was carried out using a Q-100 DSC apparatus with nitrogen as a purging gas. Samples were heated to 300 °C at a heating rate of 10 °C/min. Cyclic voltammetry (CV) was performed under N_2 using 0.1 M tetrabutylammonium hexafluorophosphate ($TBAPF_6$) in dichloromethane and was referenced to Ag/AgCl.

3. Results and Discussions

To evaluate the sensing properties and performance of our NDI-CN_4-based sensor, the sensor was initially exposed systematically to ammonia with various concentrations ranging from 3 ppm to 50 ppm, and the variations in the current intensity were recorded as a function of time. As shown in Fig. 3a, a measurable increase in the current was recorded when the sensor was exposed to 50 ppm of ammonia over a short interval of time (12.5 s). The experiment is concluded by turning off the ammonia and introducing air, leading to a shift of the current intensity back to its original level. The sensor showed high sensitivity (178%) towards 50 ppm ammonia and little variation in the current density was seen for the same gas concentrations in repeat runs. Similar effects were seen at 37.5, 25, 12.5, 6 and 3 ppm and the sensitivity plotted as a function of concentrations of ammonia, as shown in Fig. 3b, shows a very strong linear correlation. In contrast, the NDI-H_4 based sensor showed no significant response to 50 ppm ammonia (~0.2%), low baseline stability and irreproducibility as shown in Fig. 3c. These findings suggest that the presence of an electron-withdrawing group (CN) at the core positions of NDI plays a significant role in enhancing the sensing performance and its behaviour.

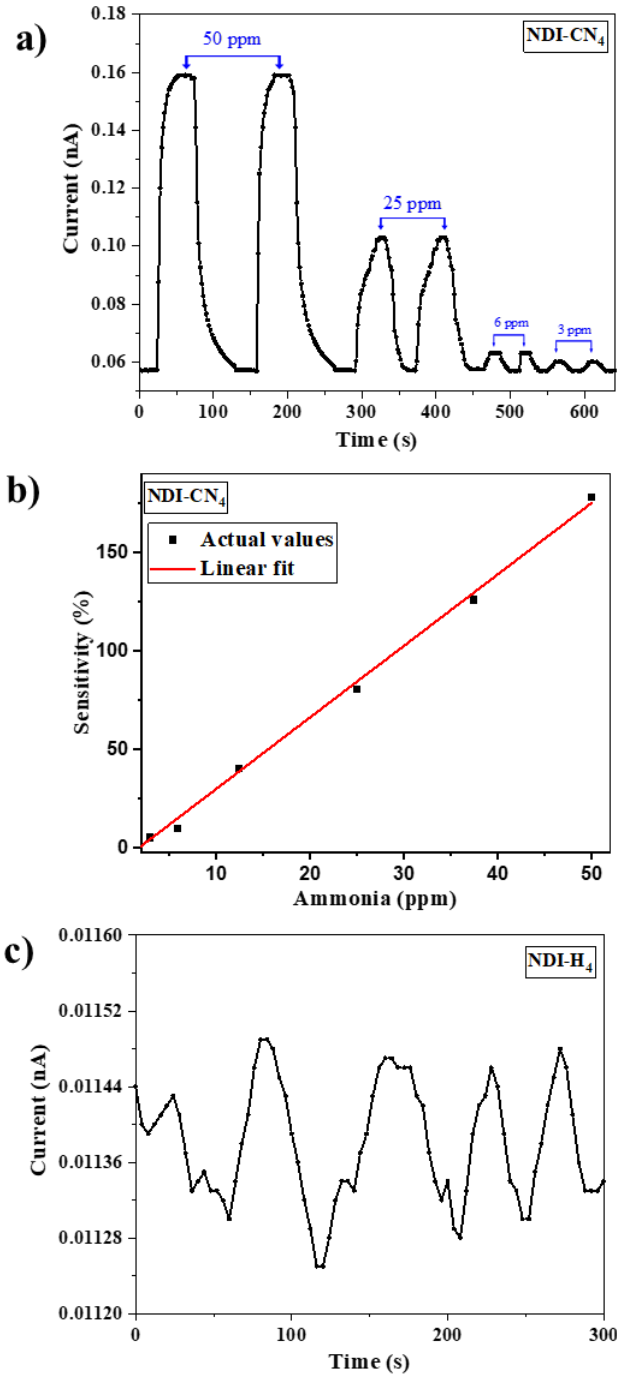

Fig. 3 (a) Dynamic response of NDI-CN_4 sensor towards ammonia with several concentrations ranging from 3 ppm to 50 ppm, (b) Sensitivity as a function of ammonia concentration, and (c) response of NDI-H_4 towards 50 ppm ammonia.

Generally, the mechanism of amperometric gas sensors based on organic semiconductor materials depends on the target gas adsorption/binding over the surface, followed by generation of charge-transfer complexes between the active layer and the target gas that dissociate and diffuse into the material sensing layer.[31] This leads to a variation in charge carriers, which, in turn, changes electrical properties, such as current or resistance. This mechanism can involve either weak, such as Van der Waals interactions, or stronger chemical interactions reliant on the chemical nature of both the target analyte and the organic semiconductor material.[32] From reported mechanisms on electrical sensors, it is generally accepted that sensing performance of organic semiconductor-based sensors is mainly associated with two important factors: (1) chemical nature of semiconductor materials, such as their redox potentials, optical band gap and molecular packing, which are related to the formation of charge carriers and its effective transport into the materials, and (2) surface area of the material, which can alter the diffusion efficiency of the analyte molecules within the layer.[24] Here, we intimate that the redox potential is playing significant role in sensing performance because of the electron-withdrawing groups attached to the core of NDI-CN_4 affects the redox properties.

The response and recovery times of any sensing device are considered crucial and a useful evaluation of the applicability of the system to use outside the laboratory. The response time is the time needed for a sensor to accomplish 90% of the overall response of the signal after exposure to target analyte, while the recovery time is the 90% of signal change to reach its baseline value after the target analyte source is turned off. The response and recovery times of the NDI-CN_4-based sensor were found to be rapid at 12.5 s and 39 s, respectively, as shown in Fig. 4a and compared to other literature systems in Table 1. To further validate the practicality of the sensor for real-world applications, the recyclability was studied by repeatedly exposing the sensor to 50 ppm of ammonia over six pulses. Similar changes in the current value were recorded after each exposure (Fig. 4b). After leaving the sensor under ambient conditions for 4 weeks, the sensor was again studied towards 50 ppm of ammonia. It is clear from Fig. 4b that the variation in sensor response post-resting gives us confidence the system exhibits outstanding reversibility and stability under continuous operation and storage conditions under ambient conditions.

The effect of relative humidity (RH) on ammonia sensing property of the NDI-CN_4-based sensor was investigated given the complications water can provide through solvation of the ammonia to any of the mechanistic considerations described earlier, and to the effect of water absorbed on the sensor surface, occupying some available ammonia adsorption sites. Fig. 4c shows the response of

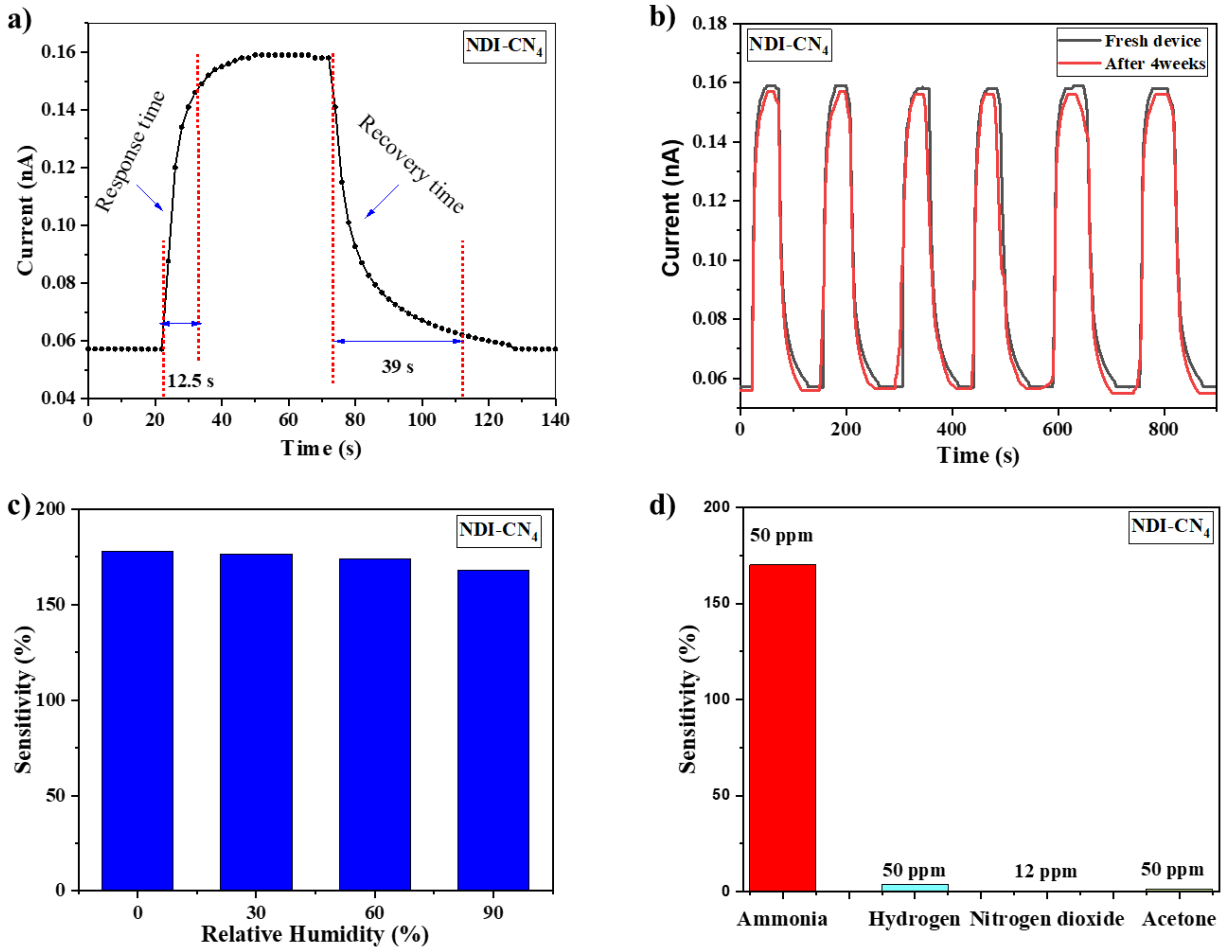

Fig. 4 (a) Response and recovery times, and (b) recyclability and long-term stability curves of the NDI-CN_4 sensor towards 50 ppm ammonia, (c) Effect of humidity on ammonia (50 ppm) sensitivity and (d) selectivity investigation.

the sensor as a function of sensitivity towards ammonia at different RH levels (0%, 30%, 60% and 90%). At low humidity levels, the ammonia response is optimal, while at higher humidity levels, it diminishes slightly due to the effect of excess water (to 94.6% of the optimum value). These results imply that the NDI-CN_4-based sensor is highly efficient in sensing ammonia under high humid conditions, thus, making it suitable for the real-life and high humid environment applications.

The selectivity of gas sensors is of prime importance for practical applications. To examine selectivity, our NDI-CN_4-based sensor was exposed to hydrogen, nitrogen dioxide and acetone as these represent reductive, oxidative, and organic vapours. To our advantage, our prototypical sensor showed a much higher response (>10×) towards ammonia when compared to other gases (Fig. 4d) which can be ascribed to stronger electrostatic interactions between ammonia and the core-extended NDI attributable to its highly electron-deficient nature.

To study the effect of surface morphology on sensing performance, the as-cast films of both NDI derivatives were analysed using AFM. The NDI-CN_4 film surface appeared amorphous with a root-mean-square (RMS) roughness of ~1 nm (Fig. 5a). On the contrary, the film surface of NDI-H_4 was found to be crystalline, a finding corroborating the physical appearance of material and the XRD analysis. The RMS roughness of NDI-H_4 film surface was ~10 nm (Fig. 5b). In this comparison, crystallinity is often an advantage to allow larger surface area on diffusive capability over smooth surfaces particularly for physisorption. However, the electronic interaction appears to dominate, yielding stronger and more stable response, and low LOD.

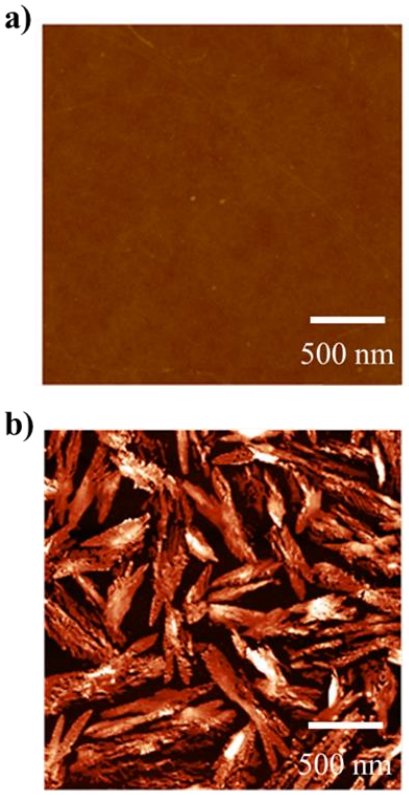

Fig. 5 AFM images for the as-cast films of (a) NDI-CN_4 and (b) NDI-H_4

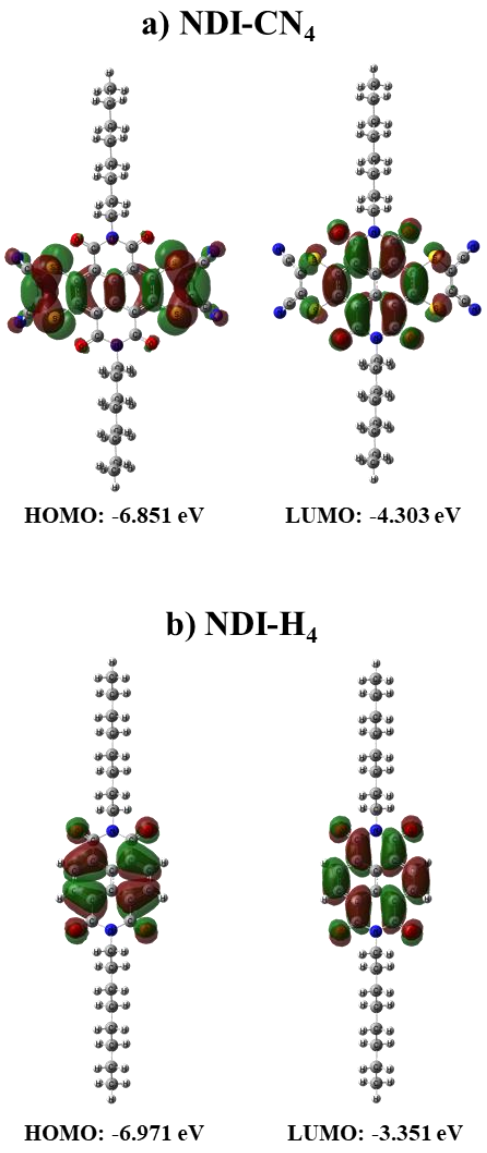

Fig. 6 The orbital density distributions for the frontier molecular orbitals of (a) NDI-CN_4 and (b) NDI-H_4

Density Functional Theory (DFT) investigations were performed to study the theoretical density distributions, i.e. the HOMO and the LUMO distributions, on the molecular backbone and were carried out through the Gaussian 09 suite of programs[33] and using B3LYP/6-31G(d) level of theory. As shown in Fig. 6a, the largest coefficients in the HOMO orbital of NDI-CN_4 are positioned on the whole lateral axis π-system, and the coefficients in the LUMO orbital are primarily located on the central NDI unit. The energy level values of the HOMO and the LUMO orbitals of NDI-CN_4 and NDI-H_4 were estimated to be; HOMO: −6.851 eV, LUMO: −4.3 eV (bandgap: 2.5 eV) and HOMO: −6.9 eV, LUMO: −3.35 eV (bandgap: 3.6 eV), respectively. As the LUMO level of NDI-CN_4 (-4.3 eV) is significantly lower than the LUMO level of NDI-H_4 (−3.6 eV), it is apparent that the former is more capable to instigate a charge transfer complex[34] with ammonia that eventually leads to the significant difference in sensitivity (178%). Thus, it can be concluded that the presence of electron-withdrawing

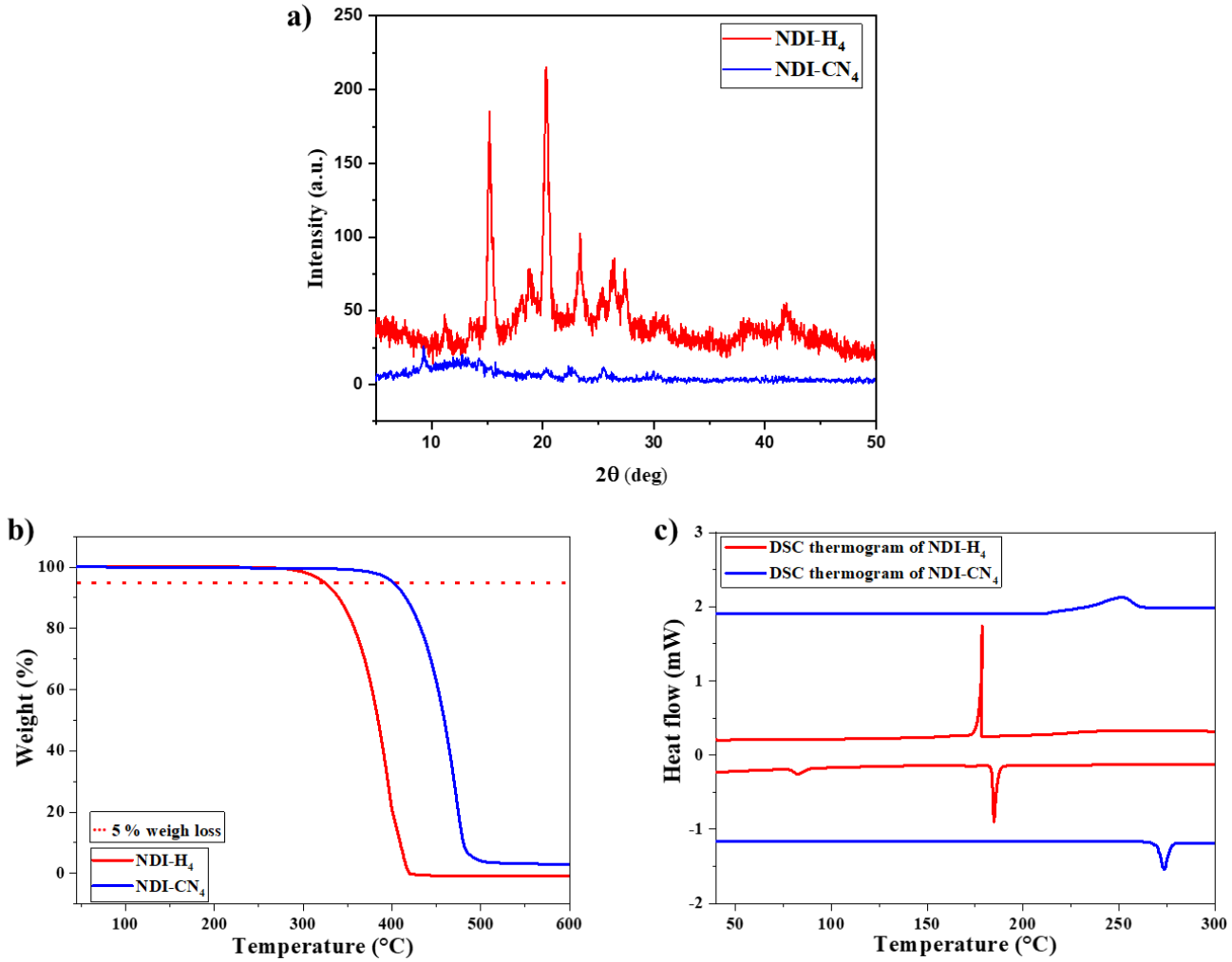

Fig. 7 (a) XRD, (b) TGA, and (c) DSC patterns comparing NDI-CN_4 and NDI-H_4.

group (-CN) in NDI-CN_4 is one of the critical factors for enhancing the sensing performance by reducing the LUMO energies that allowed the effective charge exchange between NDI-CN_4 and ammonia, making the sensor highly sensitive as well as stable. B3LYP will typically underestimate band gaps and any agreement with experiment is a fortuitous cancellation of errors. We note that range-separated functionals could be a more rigorous way to compute HOMO/LUMO levels in such systems.[35-38] Therefore, cyclic voltammetry was conducted to verify DFT results, and the details are given in Fig. S2 and Table S1.

XRD analysis of both materials in their powder (Fig. 7a) showed higher crystallinity for NDI-H_4 when compared with NDI-CN_4, a finding consistent with AFM analysis. TGA analysis of both NDI materials indicated higher thermal stability. Furthermore, NDI-CN_4 exhibited comparable high thermal stability compared to NDI-H_4, with a 5% weight-loss temperature of 402 °C (Fig. 7b). The DSC analysis (Fig. 7c) supported the high crystallinity of NDI-H_4 powder compared to NDI-CN_4 powder, with almost no glass transitions in the experimental window and sharp peaks were associated with the melting and crystallisation.

A comparative study of available ammonia sensors in the recent literature was conducted to demonstrate the advances made of NDI-CN_4-based sensor. The various sensing parameters of these sensors are depicted in Table 1. From the comparison, it can be stated that such a low-cost, highly sensitive, selective, and stable NDI-CN_4 sensor with quick response/recovery and excellent recyclability for ammonia sensing makes the current protocol highly reliable and valuable for rapid detection of ammonia.

Table 1. A comparative study of the reportable properties of NDI-CN_4-based sensor against recently reported organic semiconducting ammonia sensors at RT.

Materials	Sensor Type	T_{Res}/T_{Rec} (s)	LOD (ppm)	Response Calculation	Response	Refs.
PDI-CN_2C_{12}	Resistive	40/-	1000	$\Delta R/R_o \times 100$	40% at 1000 ppm	34
PDI-HIS	Amperometric	5/20	0.56	$\Delta I/I_o$	35 at 100 ppm	39
PDI-$LuPc_2$	Amperometric	-	10	$\Delta I/I_o$	28 at 30 ppm	40
PDIN	Amperometric	26/2	3	$\Delta I \times 100$	6.6% at 5 ppm	41
PDI-S	Amperometric	80/ -	100	I/I_o	320 at 100 ppm	42
PANi	Resistive	426/1500	5	$\Delta R/R_o \times 100$	57% at 50 ppm	43
CNTs	Resistive	300/300	100	$\Delta R/R_o \times 100$	22.5% at 100 ppm	44
Ppy-Au NPs	Resistive	-	100	$\Delta R/R_o \times 100$	1.4 at 100 ppm	45
PANI-rGO hybrid	Resistive	500/-	50	$\Delta R/R_o \times 100$	1.56 at 50 ppm	46
NDI-1	Amperometric	200/350	6.25	$\Delta I/I_o$	27.7% at 50 ppm	27
NDI-CN_4	Amperometric	12.5/39	3	$\Delta I/I_o$	178% at 50 ppm	This work

5. Conclusions

A high-performing amperometric-type sensor based on a tetracyano naphthalene diimide derivative (NDI-CN_4) was successfully fabricated, and its ammonia sensing properties were investigated in detail. The sensing parameters, such as sensitivity, selectivity, response/recovery times, recyclability, and long-term stability, were investigated and revealed exceptional sensor performance as compared with the literature. The NDI-CN_4-based sensor showed high sensing performance when compared with the sensor based on NDI-H_4, a more basic analogue of the former. The high performance of NDI-CN_4-based sensor can be primarily ascribed to the low lying LUMO level, where the strong electron withdrawing cyano groups were attached to the NDI core. These findings suggest that the core-substitutions of NDI play a major role towards the development of those target materials which can be efficiently used for gas sensing applications. The structure-function relationship investigated in this work can offer some useful information for the development of high-performing gas sensors.

Conflicts of interest

There are no conflicts to declare.

Acknowledgements

This research received funding from the Australian Renewable Energy Agency (ARENA) as part of ARENA's Research and Development Program-Renewable Hydrogen for Export (Contract No. 2018/RND012). The views expressed herein are not necessarily the views of the Australian Government, and the Australian Government does not accept responsibility for any information or advice contained herein. This research was supported by using the Nectar Research Cloud, a collaborative Australian research platform supported by the NCRIS-funded Australian Research Data Commons (ARDC). Salman Ali acknowledges the assistance of Mr Chris Harrison in sensing data collection. Salman Ali and Mohammed Jameel acknowledge PhD scholarships under the Swinburne University Postgraduate Research Award (SUPRA) and Glenn Oldham under the Australian Government Research Training Program Scheme.

References

1. M. Appl, *Future*, 1999, **245**, 12.
2. D. Kwak, Y. Lei and R. Maric, *Talanta*, 2019, **204**, 713-730.
3. H.-Y. Li, C.-S. Lee, D. H. Kim and J.-H. Lee, *ACS Appl. Mater. Interfaces.*, 2018, **10**, 27858-27867.
4. X. Zhang, B. Gu, H. van Grinsven, S. K. Lam, X. Liang, M. Bai and D. Chen, *Nat. Commun.*, 2020, **11**, 1-10.
5. P. P. Ricci and O. J. Gregory, *Sci. Rep.*, 2021, **11**, 1-7.
6. C. Malins, A. Doyle, B. MacCraith, F. Kvasnik, M. Landl, P. Šimon, L. Kalvoda, R. Lukaš, K. d. Pufler and I. Babusik, *J Environ Monit*, 1999, **1**, 417-422.
7. H.-J. Kim and J.-H. Lee, *Sens Actuators B*, 2014, **192**, 607-627.
8. M. Shafiei, F. Hoshyargar, J. Lipton-Duffin, C. Piloto, N. Motta and A. P. O'Mullane, *J. Phys. Chem. C*, 2015, **119**, 22208-22216.
9. M. Shafiei, F. Hoshyargar, N. Motta and A. P. O'Mullane, *Mater. Des.*, 2017, **122**, 288-295.
10. Y. Wang, A. Liu, Y. Han and T. Li, *Polym. Int.*, 2020, **69**, 7-17.
11. J. G. Ibanez, M. E. Rincón, S. Gutierrez-Granados, M. h. Chahma, O. A. Jaramillo-Quintero and B. A. Frontana-Uribe, *Chem. Rev.*, 2018, **118**, 4731-4816.
12. V. Schroeder, S. Savagatrup, M. He, S. Lin and T. M. Swager, *Chem. Rev.*, 2018, **119**, 599-663.
13. C. Piloto, F. Mirri, E. A. Bengio, M. Notarianni, B. Gupta, M. Shafiei, M. Pasquali and N. Motta, *Sens. Actuators B*, 2016, **227**, 128-134.
14. Z. Meng, R. M. Stolz, L. Mendecki and K. A. Mirica, *Chem. Rev.*, 2019, **119**, 478-598.
15. S. Ali, A. Gupta, M. Shafiei and S. J. Langford, *Chemosensors*, 2021, **9**, 30.
16. S. Bhosale, C H. Jani and S. J. Langford, *Chem. Soc. Rev.*, 2008, **37**, 331-342.
17. M. Jameel, T. C.-J. C.-J. Yang, G. J. Wilson, R. A. Evans, A. Gupta and S. J. Langford, *J. Mater. Chem. A*, 2021.

18. D. Sagdullina, N. Lukashkin, A. Parfenov, K. Lyssenko and P. Troshin, *Synth. Met.*, 2020, **260**, 116289.
19. F. Zhang, C. a. Di, N. Berdunov, Y. Hu, Y. Hu, X. Gao, Q. Meng, H. Sirringhaus and D. Zhu, *Adv. Mater.*, 2013, **25**, 1401-1407.
20. A. Insuasty, S. Maniam and S. J. Langford, *Chem-Eur J.*, 2019.
21. X. Gao, C.-a. Di, Y. Hu, X. Yang, H. Fan, F. Zhang, Y. Liu, H. Li and D. Zhu, *J. Am. Chem. Soc.*, 2010, **132**, 3697-3699.
22. Z. Yuan, Y. Ma, T. Geßner, M. Li, L. Chen, M. Eustachi, R. T. Weitz, C. Li and K. Müllen, *Org. Lett.*, 2016, **18**, 456-459.
23. T. He, M. Stolte and F. Würthner, *Adv. Mater.*, 2013, **25**, 6951-6955.
24. R. Song, Z. Wang, X. Zhou, L. Huang and L. Chi, *Chempluschem*, 2019, **84**, 1222-1234.
25. A. Kalita, S. Hussain, A. H. Malik, U. Barman, N. Goswami and P. K. Iyer, *ACS Appl. Mater. Interfaces.*, 2016, **8**, 25326-25336.
26. S. Ali, M. A. Jameel, A. Gupta, S. J. Langford and M. Shafiei, *Synth. Met.*, 2021, **275**, 116739.
27. S. Ali, M. A. Jameel, C. J. Harrison, A. Gupta, M. Shafiei and S. J. Langford, *Sens. Actuators B*, 2022, **351**, 130972.
28. T. Okamoto, S. Kumagai, E. Fukuzaki, H. Ishii, G. Watanabe, N. Niitsu, T. Annaka, M. Yamagishi, Y. Tani and H. Sugiura, *Sci. Adv.*, 2020, **6**, eaaz0632.
29. Y. Hu, X. Gao, C.-a. Di, X. Yang, F. Zhang, Y. Liu, H. Li and D. Zhu, *Chem. Mater.*, 2011, **23**, 1204-1215.
30. S. Maniam, S. Sandanayake, E. I. Izgorodina and S. J. Langford, *Asian J. Org. Chem.*, 2016, **5**, 490-493.
31. I. Muzikante, V. Parra, R. Dobulans, E. Fonavs, J. Latvels and M. Bouvet, *Sens.*, 2007, **7**, 2984-2996.
32. F. I. Bohrer, A. Sharoni, C. Colesniuc, J. Park, I. K. Schuller, A. C. Kummel and W. C. Trogler, *J. Am. Chem. Soc.*, 2007, **129**, 5640-5646.
33. M. Frisch, G. Trucks, H. B. Schlegel, G. E. Scuseria, M. A. Robb, J. R. Cheeseman, G. Scalmani, V. Barone, B. Mennucci and G. Petersson, *Journal*, 2009.
34. Y. Huang, L. Fu, W. Zou, F. Zhang and Z. Wei, *J. Phys. Chem. C*, 2011, **115**, 10399-10404.
35. T. Minami, M. Nakano and F. Castet, *J. Phys. Chem. Lett.*, 2011, **2**, 1725-1730.
36. M. E. Foster and B. M. Wong, *J. Chem. Theory Comput*, 2012, **8**, 2682-2687.
37. B. Mahato and A. N. Panda, *J. Phys. Chem*, 2020, **125**, 115-125.
38. B. M. Wong and T. H. Hsieh, *J. Chem. Theory Comput*, 2010, **6**, 3704-3712.
39. A. Kalita, S. Hussain, A. H. Malik, N. V. Subbarao and P. K. Iyer, *J. Mater. Chem. C*, 2015, **3**, 10767-10774.
40. P. Gaudillat, A. Wannebroucq, J.-M. Suisse and M. Bouvet, *Sens. Actuators B*, 2016, **222**, 910-917.
41. X. Wang, C. Li, Y. Huang, H. Zhai, Z. Liu and D. Jin, *Sens. Actuators B*, 2018, **275**, 451-458.
42. Q. Deng, E. Zhou, Y. Huang, W. Qing, H. Zhai, Z. Liu and Z. Wei, *Chem. Commun.*, 2019, **55**, 4379-4382.
43. N. Indarit, Y.-H. Kim, N. Petchsang and R. Jaisutti, *RSC Adv.*, 2019, **9**, 26773-26779.
44. A. G. Bannov, O. Jašek, A. Manakhov, M. Márik, D. Nečas and L. Zajíčková, *IEEE Sens. J.*, 2017, **17**, 1964-1970.
45. J. Zhang, X. Liu, S. Wu, H. Xu and B. Cao, *Sens. Actuators B*, 2013, **186**, 695-700.
46. X. Huang, N. Hu, R. Gao, Y. Yu, Y. Wang, Z. Yang, E. S.-W. Kong, H. Wei and Y. Zhang, *J. Mater. Chem.*, 2012, **22**, 22488-22495.